Nuclear Level Density and γ-ray Strength Function of ^{67}Ni and the impact on the *i*-process

V. W. Ingeberg,[1,*] S. Siem,[1,†] M. Wiedeking,[2,3] A. Choplin,[4] S. Goriely,[4] L. Siess,[4] K. J. Abrahams,[5] K. Arnswald,[6] F. Bello Garrote,[1,‡] D. L. Bleuel,[7] J. Cederkäll,[8,9] T. L. Christoffersen,[1] D. M. Cox,[10,11] H. De Witte,[12] L. P. Gaffney,[9,§] A. Görgen,[1] C. Henrich,[13] A. Illana,[12,¶] P. Jones,[2] B. V. Kheswa,[1,**] T. Kröll,[13] S. N. T. Majola,[2,**] K. L. Malatji,[2,14] J. Ojala,[10,11,§] J. Pakarinen,[10,11] G. Rainovski,[15] P. Reiter,[6] M. von Schmid,[13] M. Seidlitz,[6] G. M. Tveten,[1] N. Warr,[6] and F. Zeiser[1]

(The ISOLDE Collaboration)

[1] *Department of Physics, University of Oslo, NO-0316 Oslo, Norway*
[2] *iThemba LABS, P.O. Box 722, 7129 Somerset West, South Africa*
[3] *School of Physics, University of the Witwatersrand, 2050 Johannesburg, South Africa*
[4] *Institut d'Astronomie et d'Astrophysique, Université Libre de Bruxelles (ULB), Campus de la Plaine, CP 226, 1050 Brussels, Belgium*
[5] *Department of Physics, University of the Western Cape, P/B X17 Bellville 7535, South Africa*
[6] *Institut für Kernphysik, University of Cologne, D-50937 Cologne, Germany*
[7] *Lawrence Livermore National Laboratory, 7000 East Avenue, Livermore, California, 94550-9234, USA*
[8] *Physics Department, University of Lund, Box-118, SE-22100, Lund, Sweden*
[9] *ISOLDE, EP Department, CERN, CH-1211 Geneva, Switzerland*
[10] *Department of Physics, University of Jyväskylä, P.O. Box 35, FIN-40014 Jyväskylä, Finland*
[11] *Helsinki Institute of Physics, University of Helsinki, P.O. Box 64, FIN-00014, Helsinki, Finland*
[12] *Instituut voor Kern- en Stralingsfysica, K.U. Leuven, Celestijnenlaan 200D, B-3001 Leuven, Belgium*
[13] *Institut für Kernphysik, Technische Universität Darmstadt, D-64289 Darmstadt, Germany*
[14] *Department of Physics, Stellenbosch University, Private Bag X1, Matieland, 7602, South Africa*
[15] *Faculty of Physics, St. Kliment Ohridski University of Sofia, BG-1164 Sofia, Bulgaria*

(Dated: July 17, 2023)

Proton-γ coincidences from (d, p) reactions between a ^{66}Ni beam and a deuterated polyethylene target have been analyzed with the inverse Oslo method to find the nuclear level density (NLD) and γ-ray strength function (γSF) of ^{67}Ni. The ^{66}Ni(n,γ) capture cross section has been calculated using the Hauser-Feshbach model in `TALYS` using the measured NLD and γSF as constraints. We confirm that ^{66}Ni(n,γ) acts as a bottleneck when relying on one-zone nucleosynthesis calculations. However, we find that the impact of this reaction is strongly damped in multi-zone low-metallicity AGB stellar models experiencing i-process nucleosynthesis.

I. INTRODUCTION

The origin and production mechanism of the heavy elements has been under investigation for a long time. The first direct observations of nucleosynthesis of heavy elements was reported by P. Merrill in 1952 [1]. Soon after, the mechanism behind the production of heavy elements through neutron capture was outlined in the famous B^{2}FH paper in 1957 [2].

Nucleosynthesis beyond the Fe/Ni mass region is due to the slow neutron capture (s-process), rapid neutron capture (r-process), photo-disintegration processes, and more recent results call for an intermediate neutron capture process (i-process) [3, 4]. These processes are sensitive to nuclear properties such as the nuclear level densities (NLD) and γ-ray strength functions (γSF). The availability and uncertainties in nuclear data affect the ability to calculate reaction rates, in particular for the the r- and i-processes as they involve neutron-rich nuclei for which data is non-existing or sparse. This can have significant impact on the neutron capture rates and on the final abundance distribution of elements and their isotopes predicted by models. Currently, the vast majority of nuclei for which NLDs and γSFs have been measured lie at, or very near, the line of stability [5].

Away form stability, directly measured (n,γ) cross sections are not available and NLDs and γSFs can provide the necessary constraints. The Oslo method is particularly suitable as it extracts NLD and γSF simultaneously [6, 7]. These quantities, together with the optical model potentials, are the main ingredients in the *Hauser-Feshbach* theory [8] to calculate neutron capture cross-sections and reaction rates. The Oslo Method has been further developed using total absorption spectroscopy following β-decay leading to the β-Oslo method [9] and has demonstrated the versatility of the Oslo method and its

* vetlewi@fys.uio.no
† sunniva.siem@fys.uio.no
‡ Present address: Oslo University Hospital, NO-0424 Oslo, Norway
§ Present address: Department of Physics, University of Liverpool, L69 7ZE, United Kingdom
¶ Present address: Departamento de Estructura de la Materia, Física Térmica y Electrónica and IPARCOS, Universidad Complutense de Madrid, E-28040 Madrid, Spain
** Present address: Department of Physics, University of Johannesburg, P.O. Box 524, Auckland Park 2006, South Africa

applicability even for nuclei far from stability [9–13]. The β-Oslo method requires specific β-Q value conditions for the mother-daughter pair placing a limit on the nuclei which can be measured with this technique.

Another approach is to use inverse kinematics with radioactive beams. Here the beam intensity is the main limiting factor. Applying the Oslo method to experimental data from an inverse kinematics experiment was first demonstrated in Ref. [14] extracting the NLD and γSF of ^{87}Kr following a d(^{86}Kr, p)^{87}Kr pick-up reaction. In this paper, we have applied this inverse-Oslo method to data from a radioactive ion beam experiment to extract the NLD and γSF of ^{67}Ni. Based on these results, the neutron capture rate of ^{66}Ni was constrained using the Hauser-Feshbach theory, which is of particular importance for our understanding of the weak i-process. In the weak i-process the neutron density is large ($\sim 10^{15}$), but exposure is low due to a quick and abrupt termination of the neutron production. In such a case only the first n-capture peak elements are produced significantly [15]. This was studied in Ref. [15], where it was found that the ^{66}Ni(n, γ) reaction had a major impact on the overall production rate of heavier elements, essentially acting as a bottleneck for the entire weak i-process. Constraining the ^{66}Ni(n, γ) could improve our understanding of the i-process nucleosynthesis.

II. EXPERIMENT AND ANALYSIS

The experiment was performed using the HIE-ISOLDE facility at CERN [16], where 1.4 GeV proton beam from the PSBooster bombarded a uranium carbide target inducing fission. The evaporated fission products were ionized by the resonance ionization laser ion source (RILIS) [17] and the ^{66}Ni ions were separated by the General Purpose Separator (GPS) to be collected and cooled by a penning trap (REXTRAP) [18]. The ions were then charge bread to a 16^+ charge state by an electron-beam ion source (REXEBIS) [19, 20]. The highly ionized ^{66}Ni ions were re-accelerated by the HIE-ISOLDE linear accelerator to an energy of 4.47(1) MeV/u. The $\approx 3.5\times10^6$ pps intense ^{66}Ni beam impinged on a ≈ 670 μg/cm^2 thick secondary deuterated polyethylene target (99 % enrichment in deuterium) [21] placed at the Miniball experimental station and produced the desired d(^{66}Ni, p)^{67}Ni reactions. The total time of beam on target was approximately 140 hours. The same reaction has previously been measured at ISOLDE by Ref. [22], but used a much lower beam energy of 2.5 MeV/u. The data-set was not considered as it only reached excitation energies up to 3.5 MeV, much less than what is required for the Oslo Method.

Protons from the reaction were measured with the C-REX particle detector array [23] . Coincident γ-rays were measured using the Miniball detector array [24, 25]. Two of the eight Miniball high-purity germanium (HPGe) clusters [25] were replaced by six large-volume (3.5×8 inch) LaBr$_3$:Ce detectors to increase the high γ-ray energy efficiency of the array. Signals from the C-REX detectors were processed by an analog data acquisition system (DAQ) which fed four 32-channel analogue-to-digital converter (ADC) modules from Mesytec. The signals from the γ-ray detectors were processed by a digital DAQ consisting of XIA Digital Gamma Finders (DGF-4C). The two systems were synchronized, read out simultaneously and the data written to disk.

Prompt particle-γ coincidences were selected from the data by applying time gates on the time difference between the detected γ-rays and particles, while the (d, p) reaction was selected by applying the appropriate energy cut on the ΔE $-$ E matrix. Background events were selected in a similar fashion by placing time gates of half the size as the prompt gate on either sides of the prompt peak. This resulted in a total of 3.2×10^5 and 1.1×10^6 background subtracted proton-γ coincidences with the LaBr$_3$:Ce detectors and the Miniball clusters, respectively. The low number of proton-γ coincidences with the LaBr$_3$:Ce compared to those with the Miniball detectors is due to the lower geometric efficiency of the LaBr$_3$:Ce detectors which were located considerably further from the target. Although having only a quarter of the Miniball coincidences, the significantly higher full-energy efficiency of the LaBr$_3$:Ce include the majority of high-energy γ-ray transitions. For this reason, the results presented here are based on the analysis of proton-γ coincident events from the LaBr$_3$:Ce detectors only.

Due to the considerable residual kinetic energy of the ^{67}Ni the γ-ray energies were Doppler corrected. The maximum deflection of the residual ^{67}Ni was less than 1.5° and the maximum spread in velocity was less than 4.2% and the correction was performed using a constant factor based only on the γ-detector angle relative to the beam axis.

For each proton-γ event the excitation energy was calculated from the kinematic reconstruction of the two-body reaction. The proton-γ coincidences were collected in an excitation-γ energy matrix shown in Fig. 1(a).

Due to the Lorentz boost associated with inverse-kinematics there were no well resolved levels in the particle spectra suitable for an in-beam calibration. The particle spectra were calibrated through the gain and shift parameters which were found by performing a least squares fit of the entire $\Delta E - E$ matrix to theoretical particle energies based on the detector thickness. The calibration parameters yielded by this procedure were less precise and contributes significantly to the reduced excitation energy resolution seen in Fig. 1, although the actual contribution due to the calibration is difficult to quantify.

The first step to obtain NLDs and γSFs from excitation-γ matrices is to correct for the detector response using the unfolding method [26] by using a detector response deduced from a Geant4 [27] simulation of the experimental setup [28]. This resulted in the *unfolded* matrix shown in Fig. 1(b).

Next, an iterative subtraction method [29] is applied to

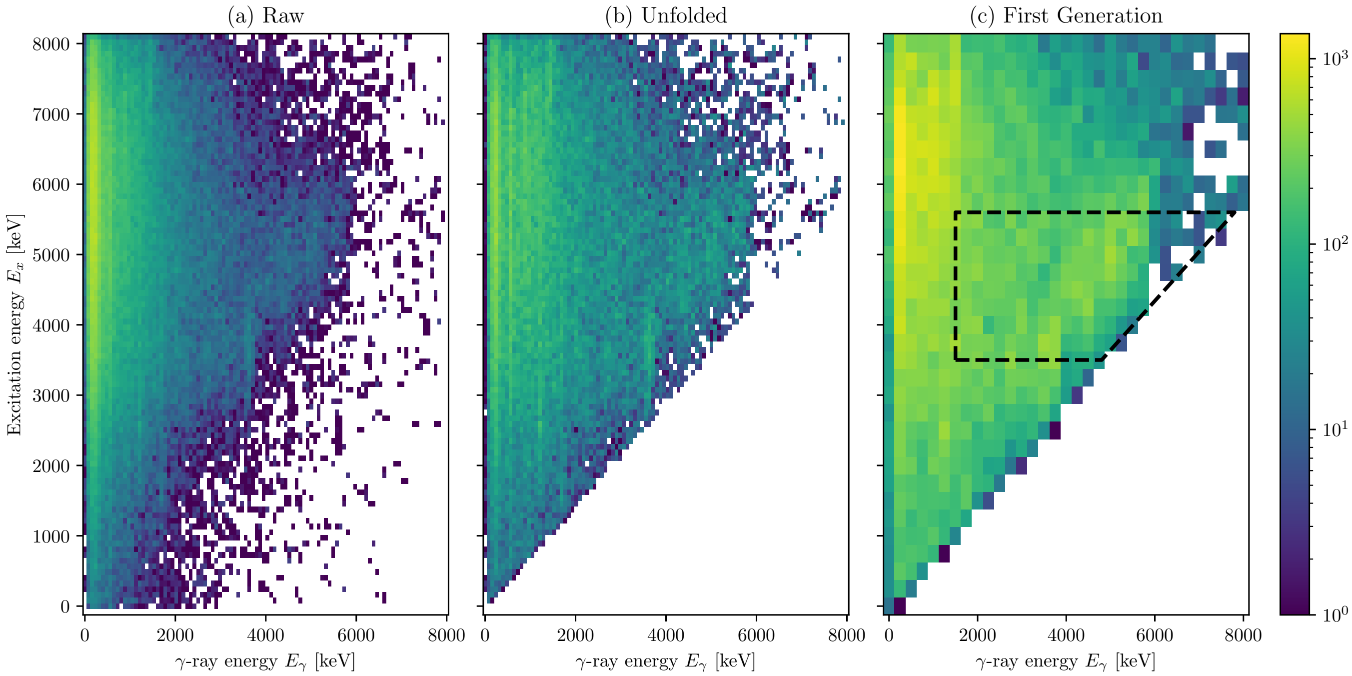

FIG. 1. Raw excitation-γ coincidence (a), unfolded (b) and first generation (c) matrices (see text for details).

the unfolded matrix in order to deduce the distribution of primary γ-rays emitted from each excitation bin, resulting in the *first generation* matrix shown in Fig. 1(c).

The first generation matrix is proportional to the γ-ray transmission coefficients $\mathcal{T}(E_\gamma)$ and the NLD $\rho(E_f = E_x - E_\gamma)$ at the final excitation energy E_f [6]

$$\Gamma(E_x, E_\gamma) \propto \mathcal{T}(E_\gamma)\rho(E_f = E_x - E_\gamma). \tag{1}$$

The NLD and transmission coefficients are extracted by normalizing the first-generation γ-ray spectra for each excitation bin and by fitting the experimental matrix with a theoretical matrix [6]

$$\Gamma_{\text{th}}(E_x, E_\gamma) = \frac{\mathcal{T}(E_\gamma)\rho(E_x - E_\gamma)}{\sum\limits_{E_\gamma = E_\gamma^{\text{min}}}^{E_x} \mathcal{T}(E_\gamma)\rho(E_x - E_\gamma)} \tag{2}$$

by minimizing

$$\chi^2 = \sum_{E_x, E_\gamma} \left(\frac{\Gamma(E_\gamma, E_x) - \Gamma_{\text{th}}(E_\gamma, E_x)}{\Delta\Gamma(E_\gamma, E_x)} \right)^2, \tag{3}$$

where $\mathcal{T}(E_\gamma)$ and $\rho(E_f = E_x - E_\gamma)$ are treated as free parameters for each γ-ray energy E_γ and final energy E_f, respectively. To ensure that only statistical transitions are considered a minimum γ-ray energy of 1.5 MeV was set. Similarly, only excitation energy bins between 3.5 and 5.6 MeV were included in the fit.

The resulting γ-ray transmission coefficients are converted to γSF by

$$f(E_\gamma) = \frac{\mathcal{T}(E_\gamma)}{2\pi E_\gamma^3}$$

under the assumption that the transmission coefficients are dominated by dipole transitions.

The theoretical first generation matrix, (2), is invariant under transformation of NLD and γSF [6]

$$\begin{aligned} \widetilde{\rho}(E_f) &= A\rho(E_f)e^{\alpha E_f} \\ \widetilde{f}(E_\gamma) &= Bf(E_\gamma)e^{\alpha E_\gamma}, \end{aligned} \tag{4}$$

where A, B and α are transformation parameters. This means that the extracted NLD and γSF do not represent the physical NLD and γSF, but contain information on the functional shape. To deduce the absolute values of the NLD and γSF the extracted NLD and γSF will have to be normalized to auxiliary data.

III. NORMALIZATION OF NLD AND γSF

Many nuclei along the island of stability have auxiliary data available with which the normalization of the NLDs and γSFs is achieved. Typical data used for this purpose are the level density from resolved discrete states, the level density at the neutron separation energy from s- and/or p-wave neutron resonance spacing data and the average radiative widths of s-wave neutron resonances. When applying the Oslo method, NLDs do not extend to the neutron separation energy as the method probes the NLD at the final excitation energy $E_f = S_n - E_\gamma$, the maximum energy possible to be considered in the first generation matrix is the neutron separation energy (depending on reaction kinematics) [30]. Hence, the measured NLDs are typically interpolated to the NLDs from resonance data at the neutron separation energy.

For nuclei where neutron resonance data are not available these have generally been estimated from systematics of nuclei in their vicinity. Neither for the case of ^{67}Ni nor for surrounding nuclei are neutron resonance data available. The situation is further aggravated by an incomplete level scheme at low excitation energies resulting in an unreliable level density of resolved discrete states. With the absence of any reliable normalization points the only practical solution for normalizing the NLD and γSF is the reliance on model estimates.

A. Bayesian analysis

Despite the lack of auxiliary data for normalization there is still valuable information on the NLD and γSF that can be obtained from the non-normalized experimental NLD and γSF. Through the application of the simple principle that the NLD increases with excitation energy places limits on the possible values of the slope parameter (α in Eq. (4)). This in turn constrains the shape of the γSF, giving valuable insight into models that can reasonably reproduce the γSF. This can be taken a step further, given a set of models for the NLD and γSF, it can be explored what the appropriate normalization and model parameters are for the best agreement between models and experimental data. To perform such an analysis we apply Bayesian statistics. Analyzing Oslo method data within a Bayesian statistics framework has previously been demonstrated by Midtbø *et al.* in Ref. [7] and our analysis is based on the framework presented therein. The starting point of the normalization analysis is Bayes' theorem

$$P(\boldsymbol{\theta}|\{\rho_i\},\{f_i\}) = \frac{\mathcal{L}(\{\rho_i\},\{f_i\}|\boldsymbol{\theta})P(\boldsymbol{\theta})}{P(\{\rho_i\},\{f_i\})}, \tag{5}$$

where $P(\boldsymbol{\theta}|\{\rho_i\},\{f_i\})$ is the posterior probability of a set of normalization and model parameters $\boldsymbol{\theta} = (A, B, \alpha, \boldsymbol{\theta}_{\mathrm{NLD}}, \boldsymbol{\theta}_{\gamma\mathrm{SF}})$, given a set of non-normalized NLD points $\{\rho_i\}$ and γSF points $\{f_i\}$. The likelihood $\mathcal{L}(\{\rho_i\},\{f_i\}|\boldsymbol{\theta})$ is the probability of measuring non-normalized NLD and γSF given the set of parameters $\boldsymbol{\theta}$. $P(\boldsymbol{\theta})$ is the prior probability of a set of normalization and model parameters. The evidence $P(\{\rho_i\},\{f_i\})$ is the probability of measuring the non-normalized NLD and γSF. With the assumption of Gaussian distributed uncertainties of the measured non-normalized NLD and γSF leads to the likelihood

$$\mathcal{L}(\boldsymbol{\theta}) = \prod_i \mathcal{L}_i(\boldsymbol{\theta}), \tag{6}$$

with

$$\ln \mathcal{L}_{\mathrm{discrete}} = \sum_j \ln \frac{1}{\sqrt{2\pi}\sigma_{\rho_j,\mathrm{Oslo}}(\boldsymbol{\theta})} - \frac{1}{2}\sum_j \left(\frac{\rho_{j,\mathrm{discrete}} - \rho_{j,\mathrm{Oslo}}(\boldsymbol{\theta})}{\sigma_{\rho_j,\mathrm{Oslo}}(\boldsymbol{\theta})}\right)^2, \tag{7}$$

$$\ln \mathcal{L}_{\mathrm{NLD}} = \sum_j \ln \frac{1}{\sqrt{2\pi}\sigma_{\rho_j,\mathrm{Oslo}}(\boldsymbol{\theta})} - \frac{1}{2}\sum_j \left(\frac{\rho_{j,\mathrm{model}}(\boldsymbol{\theta}) - \rho_{j,\mathrm{Oslo}}(\boldsymbol{\theta})}{\sigma_{\rho_j,\mathrm{Oslo}}(\boldsymbol{\theta})}\right)^2, \tag{8}$$

$$\ln \mathcal{L}_{\gamma\mathrm{SF}} = \sum_j \ln \frac{1}{\sqrt{2\pi}\sigma_{f_j,\mathrm{Oslo}}(\boldsymbol{\theta})} - \frac{1}{2}\sum_j \left(\frac{f_{j,\mathrm{model}}(\boldsymbol{\theta}) - f_{j,\mathrm{Oslo}}(\boldsymbol{\theta})}{\sigma_{f_j,\mathrm{Oslo}}(\boldsymbol{\theta})}\right)^2, \tag{9}$$

$$\ln \mathcal{L}_{^{68}\mathrm{Ni}} = -\frac{1}{2}\sum_j \left(\frac{f_{j,\mathrm{model}}(\boldsymbol{\theta}) - f_{j,^{68}\mathrm{Ni}}(\boldsymbol{\theta})}{\sigma_{j,^{68}\mathrm{Ni}}}\right)^2. \tag{10}$$

Here, $\mathcal{L}_{\mathrm{discrete}}$ represents the likelihood of measuring a set of NLDs given the known level density from discrete levels $\rho_{j,\mathrm{discrete}}$, $\mathcal{L}_{\mathrm{NLD}}$ is the likelihood given a specific NLD model and $\mathcal{L}_{\gamma\mathrm{SF}}$ is the likelihood given a γSF. The $\mathcal{L}_{^{68}\mathrm{Ni}}$ likelihood is included to further constrain the γSF using the measured γSF in ^{68}Ni as the γSF above the neutron separation energy are typically very similar in neighboring nuclei. Further discussion on models and parameter priors will follow in Sect. III B and Sect. III C, respectively. $\rho_{j,\mathrm{Oslo}}(\boldsymbol{\theta})$, ($f_{j,\mathrm{model}}(\boldsymbol{\theta})$) and $\sigma_{\rho_j,\mathrm{Oslo}}((\boldsymbol{\theta})$ ($\sigma_{f_j,\mathrm{Oslo}}(\boldsymbol{\theta})$) are the normalized NLD (γSF) and standard deviation, given a set of normalization parameters $A, B, \alpha \in \boldsymbol{\theta}$, respectively (see Eq. 4).

Instead of NLDs from resolved discrete states we have considered level densities based on the counting of levels from large-scale shell model (SM) calculations of ref. [31]. For shell model results utilizing the `ca48mh1g` interaction, see Refs.[10, 31] for details. Justification for this choice is based on the comparison between known low-lying levels and shell model results of other Ni isotopes [10]. These are shown to reproduce experimental NLDs with reasonable accuracy, see .

To perform the actual Bayesian analysis, model and normalization parameters were sampled using the Bayesian nested sampling algorithm `MulitNest` [32–34] in the `PyMultinest` package [35]. Final, model-dependent, normalized NLD and γSF are obtained by averaging the posterior for each combination of NLD and γSF model.

B. Models

A total of three NLD models and four γSF models have been considered, making the total number of inferred posteriors twelve. In this section we will describe the models considered.

NLD

For energies above the point where the model space of the shell model calculation is exhausted the NLD has been modeled with three different models. These include the BSFG model [36, 37]

$$\rho_{\mathrm{BSFG}}(E_x) = \frac{\sqrt{\pi}}{12\sigma}\frac{\exp(2\sqrt{a(E_x-\delta)})}{a^{1/4}(E_x-\delta)^{5/4}}, \quad (11)$$

where a is the level density parameter, δ is the energy shift and σ is the spin-cutoff parameter. The CT model [38]

$$\rho_{\mathrm{CT}}(E_x) = \frac{1}{T}e^{\frac{E_x-\delta}{T}}, \quad (12)$$

where T is the nuclear temperature and δ is an energy shift parameter. Lastly, tabulated Hartree-Fock-Bogoliubov (HFB) calculations [39] were also considered, and allowed to be re-normalized through

$$\rho_{\mathrm{HFB}}(E_x) = \hat{\rho}_{\mathrm{HFB}}(E_x-\delta)e^{c\sqrt{E_x-\delta}}, \quad (13)$$

where again δ is used to denote an energy shift, c is a slope parameter and $\hat{\rho}_{\mathrm{HFB}}$ are the tabulated NLDs. It should be noted that δ in eqs. (11), (12), and (13) are not the same parameters and will be sub-scripted whenever there is ambiguity which parameter is being referenced. The spin distribution for the BSFG and CT models was given by the Ericson distribution [36, 38]

$$g(E_x,J) = \exp\left(-\frac{J^2}{2\sigma^2(E_x)}\right) - \exp\left(-\frac{(J+1)^2}{2\sigma^2(E_x)}\right), \quad (14)$$

with the spin-cutoff parameterized by [40, 41]

$$\sigma^2(E_x) = \begin{cases} \sigma_d^2 & E < E_d \\ \sigma_d^2 + \frac{E-E_d}{S_n-E_d}(\sigma^2(S_n)-\sigma_d^2) & E \geq E_d, \end{cases} \quad (15)$$

where the spin distribution is constant at energies less than $E_d = 2.0$ MeV.

γSF

For the γSF we have considered the Simplified version of the Modified Lorentzian model (SMLO) [42] and the microscopic Gogny-HFB plus quasi-particle random phase approximation (Gogny-HFB+QRPA) with phenomenological corrections [43]. The SMLO model describes the γSF with the giant dipole resonance (GDR) for downward strength is given by

$$\begin{aligned} f_{\mathrm{GDR}}(E_\gamma) = &\frac{1}{3\pi^2\hbar^2c^2}\frac{\sigma_{\mathrm{TRK}}}{1-\exp(-E_\gamma/T)} \\ &\times\frac{2}{\pi}\frac{E_\gamma\Gamma(E_\gamma,T)}{(E_\gamma^2-E_{\mathrm{GDR}}^2)^2+E_\gamma^2\Gamma^2(E_\gamma,T)}, \end{aligned} \quad (16)$$

where E_{GDR} is the centroid of the GDR, $\sigma_{\mathrm{TRK}} = 60\frac{NZ}{A}$ is the Thomas-Reiche-Kuhn sum rule [42] and T is the temperature at the final excitation energy. The width,

$$\Gamma(E_\gamma,T) = \frac{\Gamma_{\mathrm{GDR}}}{E_{\mathrm{GDR}}}\left(E_\gamma + \frac{(2\pi T)^2}{E_{\mathrm{GDR}}}\right), \quad (17)$$

depends on the final temperature and the Γ_{GDR} which is the width found in the upward strength function. Within the SMLO model the M1 strength is parameterized as two standard Lorentzians (SLO)

$$f_{\mathrm{SLO}}(E_\gamma) = \frac{1}{3\pi^2\hbar^2c^2}\frac{E_\gamma\Gamma^2}{(E_\gamma^2-E_r^2)^2+(E_\gamma\Gamma)^2} \quad (18)$$

for the scissors and the spin-flip resonances. The low-energy upbend is modeled as a simple exponential [39]. From the shape of the non-normalized γSF there are no obvious signs of a scissors resonance which is consistent with the relatively low estimated axial deformation of $\beta_2 =\ 0.05$ [44] and has been omitted from further consideration in the model for the γSF. The assumed M1 strength contributions are thus

$$f_{\mathrm{M1}}(E_\gamma) = f_{\mathrm{SLO}}(E_\gamma, E_{\mathrm{sf}}, \Gamma_{\mathrm{sf}}, \sigma_{\mathrm{sf}}) + C\exp(-\eta E_\gamma), \quad (19)$$

where E_{sf} is the mean energy, Γ_{sf} is the width and σ_{sf} the cross-section of the spin-flip resonance. The slope of the upbend is η, C the zero-limit and the assumption of M1 strength is based on results from shell model calculations [45–48].

In the second model, the Gogny-HFB+QRPA model, the downward E1 strength is given by

$$\begin{aligned} f_{\mathrm{E1}}(E_\gamma) = &c_{\mathrm{E1}}f_{\mathrm{E1}}^{\mathrm{QRPA}}(E_\gamma-\delta_{\mathrm{E1}}) \\ &+\frac{f_0U}{1+\exp(E_\gamma-\epsilon_0)}, \end{aligned} \quad (20)$$

where $f_{\mathrm{E1}}^{\mathrm{QRPA}}(E_\gamma)$ is the strength found in Gogny-HFB+QRPA calculations. The phenomenological parameters f_0, ϵ_0 are free parameters and U is the excitation energy of the initial level. The strength are allowed to be scaled and shifted through the parameters c_{E1} and δ_{E1}, respectively. The M1 strength was estimated within the SMLO model (eq. (19)).

Data points from a Coulomb dissociation measurement of ^{68}Ni are also considered [49]. This features a strong narrow Pygmy dipole resonance at $E_x \approx 9.5$ MeV which has been accounted for by including a SLO in the E1 strength. Since the extracted γSF in ^{67}Ni only extends to 5.8 MeV we cannot determine if such a PDR also exists in ^{67}Ni. In order to account for either possibility, we have repeated the analysis both with and without the PDR. In the latter case the two lowest points of ^{68}Ni were excluded in the likelihood (Eq. (10)).

C. Parameter priors

A list of all model combinations and their parameters are listed in Table I.

TABLE I. List of all NLD and γSF models considered and their parameters.

Model	$\boldsymbol{\theta}_{\mathrm{NLD}}$	$\boldsymbol{\theta}_{\gamma\mathrm{SF}}$
CT+SMLO	T, δ_{CT}, σ_d, $\sigma(S_n)$	E_{GDR}, Γ_{GDR}, σ_{GDR}, E_{sf}, Γ_{sf}, σ_{sf}, C, η
CT+SMLO+PDR	T, δ_{CT}, σ_d, $\sigma(S_n)$	E_{GDR}, Γ_{GDR}, σ_{GDR}, E_{PDR}, Γ_{PDR}, σ_{PDR}, E_{sf}, Γ_{sf}, σ_{sf}, C, η
CT+HFB-QRPA	T, δ_{CT}, σ_d, $\sigma(S_n)$	c_{E1}, δ_{E1}, f_0, ϵ_0, E_{sf}, Γ_{sf}, σ_{sf}, C, η
CT+HFB-QRPA+PDR	T, δ_{CT}, σ_d, $\sigma(S_n)$	c_{E1}, δ_{E1}, f_0, ϵ_0, E_{PDR}, Γ_{PDR}, σ_{PDR}, E_{sf}, Γ_{sf}, σ_{sf}, C, η
BSFG+SMLO	a, δ_{BSFG}, σ_d, $\sigma(S_n)$	E_{GDR}, Γ_{GDR}, σ_{GDR}, E_{sf}, Γ_{sf}, σ_{sf}, C, η
BSFG+SMLO+PDR	a, δ_{BSFG}, σ_d, $\sigma(S_n)$	E_{GDR}, Γ_{GDR}, σ_{GDR}, E_{PDR}, Γ_{PDR}, σ_{PDR}, E_{sf}, Γ_{sf}, σ_{sf}, C, η
BSFG+HFB-QRPA	a, δ_{BSFG}, σ_d, $\sigma(S_n)$	c_{E1}, δ_{E1}, f_0, ϵ_0, E_{sf}, Γ_{sf}, σ_{sf}, C, η
BSFG+HFB-QRPA+PDR	a, δ_{BSFG}, σ_d, $\sigma(S_n)$	c_{E1}, δ_{E1}, f_0, ϵ_0, E_{PDR}, Γ_{PDR}, σ_{PDR}, E_{sf}, Γ_{sf}, σ_{sf}, C, η
HFB+SMLO	c_{HFB}, δ_{HFB}	E_{GDR}, Γ_{GDR}, σ_{GDR}, E_{sf}, Γ_{sf}, σ_{sf}, C, η
HFB+SMLO+PDR	c_{HFB}, δ_{HFB}	E_{GDR}, Γ_{GDR}, σ_{GDR}, E_{PDR}, Γ_{PDR}, σ_{PDR}, E_{sf}, Γ_{sf}, σ_{sf}, C, η
HFB+HFB-QRPA	c_{HFB}, δ_{HFB}	c_{E1}, δ_{E1}, f_0, ϵ_0, E_{sf}, Γ_{sf}, σ_{sf}, C, η
HFB+SMLO+PDR	c_{HFB}, δ_{HFB}	c_{E1}, δ_{E1}, f_0, ϵ_0, E_{PDR}, Γ_{PDR}, σ_{PDR}, E_{sf}, Γ_{sf}, σ_{sf}, C, η

To select the priors for the normalization parameters A, B and α, an approximate solution was first found by calculating the maximum-likelihood estimator (MLE) $\hat{\theta}$ by minimizing the likelihood (Eq. (6)). Both A and B are assumed to have a Gaussian prior distribution truncated at zero (negative values are nonphysical) with the mean μ given by MLE with width $\sigma = 10\mu$. The slope parameter α has a Gaussian prior distribution with mean μ again given by MLE but with a width of 1 $\sigma = 1$ MeV^{-1}.

For the model parameters the priors were represented as either Gaussians or truncated Gaussians for the physical or nonphysical values, respectively. For the NLD models fairly weak informed priors were used. In the case of the BSFG model the level density parameter a mean value of $\mu = 8.2$ MeV was selected as the approximate mean of the systematics from Refs. [37, 50], Refs. [51, 52] and Ref. [52] with width $\sigma = \mu$. The shift parameter δ_{BSFG} is a Gaussian with $\mu = 0$ MeV and $\sigma = 10$ MeV. Similarly the CT model priors were selected from the systematics of Ref. [52] with widths of $\sigma = 2$ MeV for the temperature and $\sigma = 10$ MeV for the shift parameter δ_{CT}. The slope and shift parameters c and δ_{HFB} for the HFB was centered around 0 MeV$^{-1/2}$ and 0 MeV, respectively with a width of 1 MeV$^{-1/2}$ and 1 MeV, respectively. The discrete spin-cutoff parameter $\sigma_d = 2.50(25)$ was found by examining the tabulated shell model levels while the spin-cutoff at the neutron separation energy is $\sigma(S_n) = 3.80(38)$ from an average of spin-cut off models in [37, 39, 51]. In both cases an uncertainty of 10% was assumed. The priors for all NLD model parameters are listed in Table II.

The parameters for the SMLO model were taken from the systematics in [42]. Unless an uncertainty was provided it was assumed to be 10%. The scale c_{E1} and shift δ_{E1} for the Gogny-HFB+QRPA was assumed to be centered around 1 and 0 MeV, respectively, with a width of 0.5 MeV for both. The phenomenological parameters f_0 and ϵ_0 are taken from [43]. The spin-flip and upbend parameters were taken from [42] assuming 10% uncertainty, except for C, where the width was assumed to be the same as the mean. Lastly, the PDR parameters were taken from [49]. All priors parameters related to the γSF models are listed in Table III.

TABLE II. Gaussian model parameter priors used for the extrapolation of the NLD between the experimental points and the neutron separation energy.

Parameter	μ	σ
a	8.2 MeV	8.2 MeV
δ (BSFG)	0 MeV	10 MeV
T	0.958 MeV	2 MeV
δ (CT)	-0.359 MeV	10 MeV
c (HFB)	0 MeV$^{-1/2}$	1 MeV$^{-1/2}$
δ (HFB)	0 MeV	1 MeV
σ_d	2.5	0.25
$\sigma(S_n)$	3.8	0.38

TABLE III. Model parameter priors used for the γSF models extrapolated to the extracted γSF of ^{67}Ni.

Parameter	μ	σ
E_{GDR}	17.68 MeV	0.19 MeV
Γ_{GDR}	6.0 MeV	2.8 MeV
σ_{GDR}	978 mb MeV	98 mb MeV
c_{E1}	1	0.5
δ_{E1}	0 MeV	0.5 MeV
f_0	2.5×10^{-10} MeV^{-4}	2.5×10^{-10} MeV^{-4}
ϵ_0	4 MeV	1 MeV
E_{PDR}	9.55 MeV	0.17 MeV
Γ_{PDR}	1.02	0.26 MeV
σ_{PDR}	27.4 mb	5.6 mb
E_{sf}	8.93 MeV	0.90 MeV
Γ_{sf}	4.0 MeV	0.4 MeV
σ_{sf}	1.0 mb	0.1 mb
C	3.5×10^{-8} MeV^{-3}	3.5×10^{-8} MeV^{-3}
η	0.8 1/MeV	0.08 1/MeV

D. Results

The resulting normalized NLD and γSF are shown in Figs. 2 and 3. Neither the inclusion nor exclusion of the PDR has a noticeable effect on the normalized NLD, while the effect was minimal on the γSF, see Fig. 4. The NLD and γSF is therefore averaged over all model combinations.

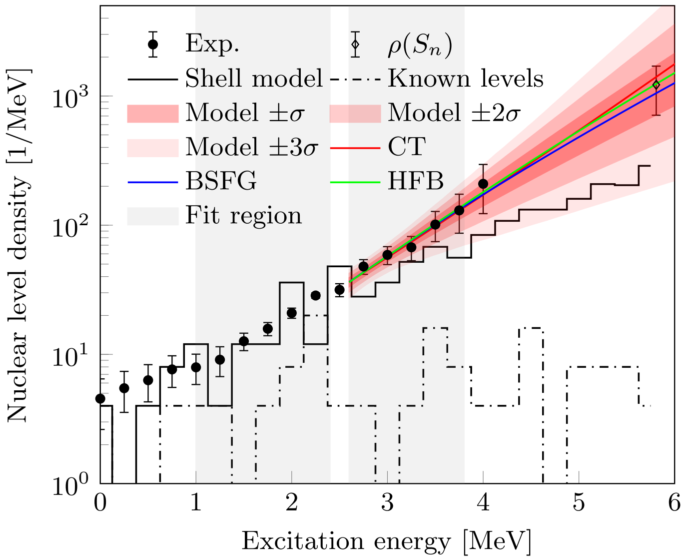

FIG. 2. The measured nuclear level density of ^{67}Ni is shown by the black circles while the black line shows the NLD from large scale SM calculations of [31]. The black dash-dotted line shows the NLD from known discrete levels [53, 54]. The red, blue and green lines show the average for the CT, BSFG and HFB models, respectively. The red shaded area indicates the $\pm1\sigma$, $\pm2\sigma$ and $\pm3\sigma$ credibility intervals. The black triangle shows the NLD at the neutron separation energy.

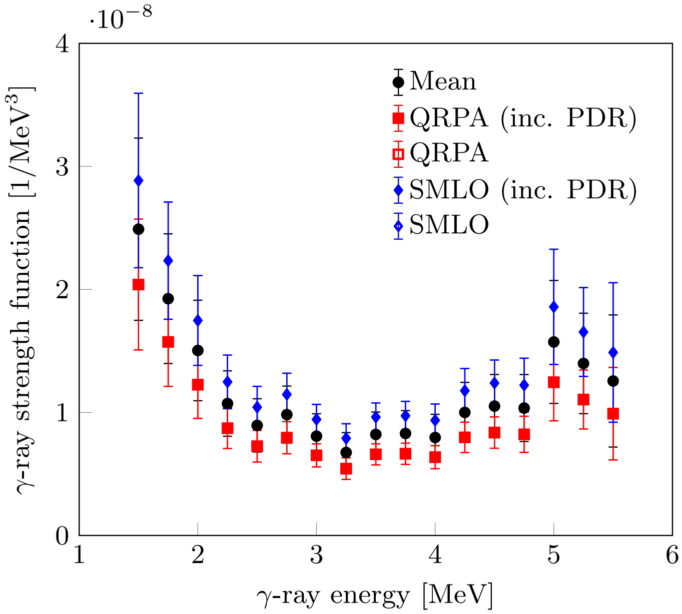

FIG. 4. Comparison of the various γSF normalizations including and excluding the PDR. The black circles shows the average normalized γSF.

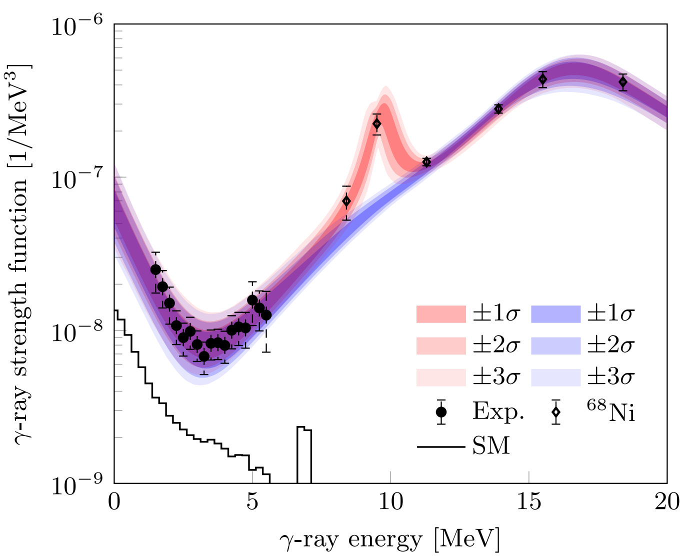

FIG. 3. The measured γ-ray strength function of ^{67}Ni is shown by the black circles while the black line shows the M1-strength found in large scale SM calculations from [31]. The red and blue shaded area indicates the $\pm1\sigma$, $\pm2\sigma$ and $\pm3\sigma$ credibility intervals for the models including the PDR and the models excluding the PDR, respectively. The black diamonds are the γSF data of ^{68}Ni measured by Rossi *et al.* [49].

IV. HAUSER-FESHBACH CALCULATIONS

The measured NLD and γSF in ^{67}Ni were used in Hauser-Feshbach calculations to constrain the neutron capture cross section of ^{66}Ni. From each posterior sample of normalization and model parameters tabulated NLD and γSF values were generated from linear interpolation and used as input to the `TALYS`[1] reaction code [55]. Since the level scheme of ^{67}Ni is far from complete only the first two discrete levels were used in the Hauser-Feshbach calculations, while above those the measured NLD was used.

In Fig. 5, the average of all calculated capture cross sections, based on the experimental data, is shown together with the `TALYS` default input and calculations with all combinations of NLD and γSF models as implemented in `TALYS`. Fig. 5 also includes results from the TENDL [56], and JEFF-3.3 [57] evaluations.

V. DISCUSSION

The Oslo method relies on external nuclear data for the normalization. In the absence of those, additional uncertainties may be induced and model dependencies may become significant. This is apparent through the relatively large uncertainties toward S_n on the measured NLD for ^{67}Ni.

The challenge specific to inverse kinematic reactions is the Lorentz boost which causes a strong angular de-

[1] Version 1.96

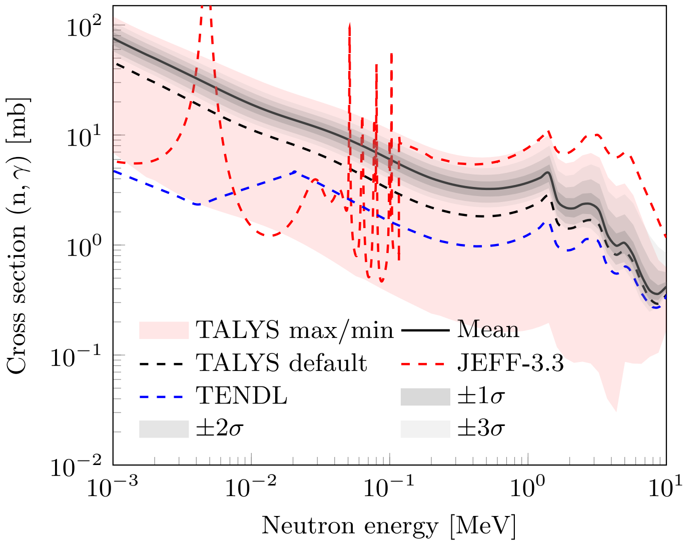

FIG. 5. The mean calculated capture cross section from the sampled NLD and γSF are given by the black line. The gray shaded area shows the $\pm1\sigma$, $\pm2\sigma$ and $\pm3\sigma$ credibility intervals. The black dashed line are the capture cross section with TALYS default values. The red shaded area shows the upper and lower limit based on all NLD and γSF models available in TALYS. The red and blue dashed lines shows the JEFF-3.3 library [57] and the TENDL library [56], respectively.

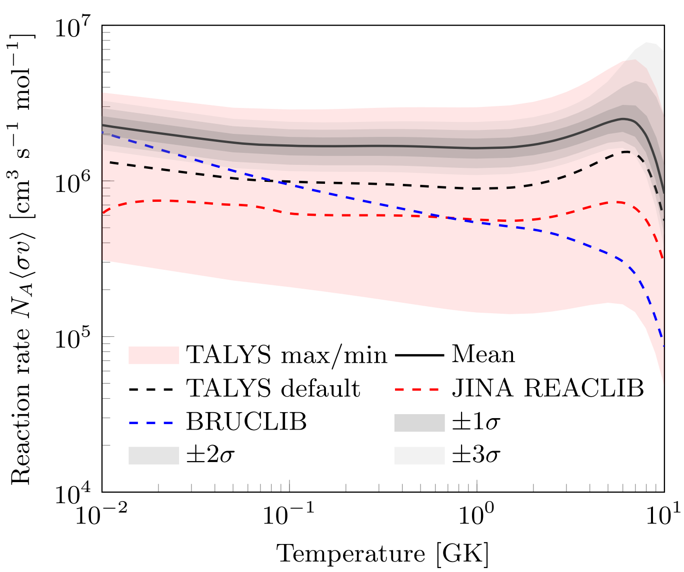

FIG. 6. The mean calculated capture rate from the sampled NLD and γSF are given by the black line. The gray filled area shows the $\pm1\sigma$, $\pm2\sigma$ and $\pm3\sigma$ credibility intervals. The black dashed line are the capture rate with TALYS default. The red and blue dashed lines are the reaction rates from JINA REACLIB v1.1 [58] and BRUCLIB [59], respectively. The red shaded area shows the upper and lower limit based on the NLD and γSF models included in the uncertainty estimation of Ref. [15].

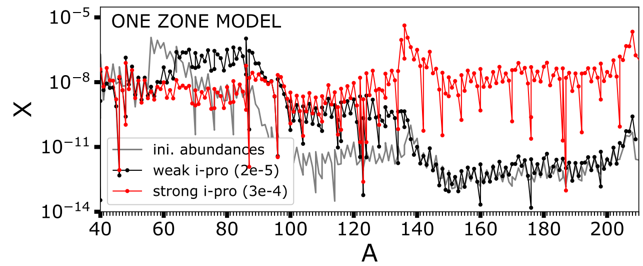

FIG. 7. Final nuclei mass fractions (after decays) as a function of mass number after a weak (black) and a strong (red) i-process using the one-zone model. The initial proton mass fraction is indicated in parenthesis (see text for details). The grey pattern shows the initial abundances.

pendence in the kinematic reconstruction of the residual excitation energy. This leads to an excitation-energy resolution which is limited by the angular opening of the particle telescope's active areas. The consequences are most apparent in the NLD where very little structures are visible.

In contrast, the measured γSF still retains noticeable features and clearly exhibits a well established enhancement for $E_x < 4$ MeV similar to those found in other Ni isotopes [10, 60–64]. Its observation indicates that the upbend is a structure which exists also away from stability. The upbend in ^{67}Ni is predicted to be due to M1 strength, based on large-scale shell model calculations [31], and shown by the black solid line in Fig. 3. The significant strength in the enhancement and the simultaneous absence of a measurable scissors resonance may be supportive of the suggested connection of the two structures [46, 65], although results on the γSF in $^{142,144-151}$Nd seem to contradict this [66].

The calculated ^{66}Ni(n,γ) capture cross section in Fig. 5 features an uncertainty of $\approx$ 40%, constraining the cross section considerably. It is interesting to note that our cross section, lies consistently higher than the recommended values as provided in TALYS, JENDEL-5, and TENDL but is smaller than the JEFF 3.3 for $E_n > 100$ keV. These differences highlight the necessity for measurements of NLDs and γSFs, especially for nuclei away from stability.

In Ref. [15] the capture rate was allowed to vary within a factor of 10 and is significantly constrained by our results, as shown in Fig. 6. Our results shows that the reaction rate is rather high compared with the rate used in Ref. [15]. This suggests a short exposure time for the weak i-process, and could help pinpoint details in the stellar environment responsible for the production of neutrons.

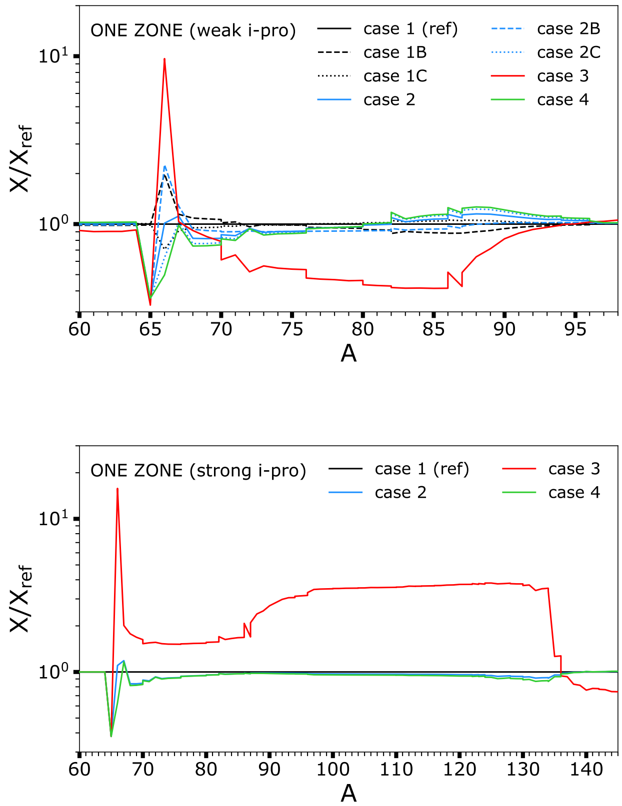

FIG. 8. Final nuclei mass fractions (after decays) as a function of mass number after a weak (top panel) and a strong (bottom) i-process using the one-zone model. The abundances are normalized by the abundances of the case 1. The 8 cases correspond to the 8 different combinations of rates indicated in Table IV (cases 1B, 1C, 2B and 2C are not shown in the bottom panel for clarity).

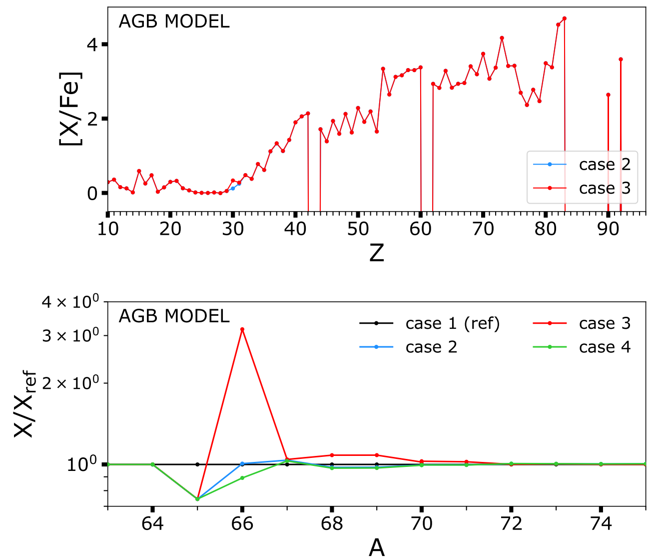

FIG. 9. Final surface abundances (after decays) for a full AGB stellar model. Top: [X/Fe] ratios, defined as $[X/Fe] = \log_{10}(N_X/N_{Fe})_\star - \log_{10}(N_X/N_{Fe})_\odot$ with N_X the number density of an element X. The first and second $\log_{10}$ terms refer to the abundances of the model and the Sun, respectively. Bottom: same as Fig. 8. The 4 cases correspond to the 4 different combinations of rates indicated in Table IV.

VI. ASTROPHYSICAL IMPLICATIONS

The ^{66}Ni(n,γ) capture rate was suggested to be of key importance for the overall production of heavy elements during the i-process nucleosynthesis taking place in Sakurai's object or rapidly accreting white dwarfs [15]. One possible astrophysical site with similar i-process conditions are low-metallicity low-mass stars during the early thermally pulsating Asymptotic Giant Branch (AGB) phase [67–71]. During this stage, protons can be engulfed by the convective thermal pulse. As they are transported downwards by convection in a timescale of about 1 hr, they are burnt rapidly by ^{12}C$(p,\gamma)^{13}$N. After the decay of ^{13}N to ^{13}C in about 10 min, the reaction ^{13}C(α,n) is activated at the bottom of the thermal pulse and leads to neutron densities of up to $\sim 10^{15}$ cm^{-3}. Stellar modeling was performed with the stellar evolution code STAREVOL [72–74]. A 1 $M_\odot$ AGB model at a metallicity of [Fe/H] $= -2.5$ is considered. This model is discussed in detail in Ref. [71].

We estimated the impact of the new ^{66}Ni(n,γ) rate on the i-process nucleosynthesis in these objects. The effects are evaluated on both multi-zone stellar evolution models and in one-zone nucleosynthesis calculations. We used a reaction network including 1160 nuclei, linked through 2123 nuclear reactions (n-, p-, α-captures and α-decays) and weak interactions (electron captures, β-decays). Nuclear reaction rates were taken from BRUSLIB, the Nuclear Astrophysics Library of the Université Libre de Bruxelles[2] [59] and the updated experimental and theoretical rates from the NETGEN interface [75]. Additional details can be found in Refs. [71, 76, 77]. In our sensitivity analysis, eight cases were investigated. We consider, for the ^{66}Ni(n,γ) reaction, the recommended Maxwellian-averaged cross section (MACS) from this work (10.7 ± 5 mb at 30 keV) as well as the minimum (1 mb at 30 keV) and maximum (19 mb at 30 keV) rates predicted by a global unconstrained TALYS calculation. Additionally, the rate of ^{65}Ni(n,γ) was also varied because ^{65}Ni has a half-life of ~ 2.5 hr (55 hr for ^{66}Ni), which is fast enough to partially bypass the neutron capture during the i-process. For ^{65}Ni(n,γ), we considered the minimum (10 mb at 30 keV) and maximum (70 mb at 30 keV) MACS predicted by TALYS for different NLD and γSF models. We also considered the uncertainties related to the nominal ^{66}Ni(n,γ) MACS evaluated in this

[2] Available at http://www.astro.ulb.ac.be/bruslib/

TABLE IV. The different cases considered for the rates of ^{65}Ni(n,γ) and ^{66}Ni(n,γ) for the one-zone and stellar model calculations.

	^{65}Ni(n,γ)	^{66}Ni(n,γ)
case 1	TALYS min	nominal
case 1B	TALYS min	nominal -5 mb
case 1C	TALYS min	nominal $+5$ mb
case 2	TALYS max	nominal
case 2B	TALYS max	nominal -5 mb
case 2C	TALYS max	nominal $+5$ mb
case 3	TALYS max	TALYS min
case 4	TALYS max	TALYS max

study by varying it by ± 5 mb at 30 keV (cases 1B, 1C, 2B and 2C). The different cases considered are reported in Table IV.

The initial abundances of the one-zone model correspond to the chemical composition in the thermal pulse of the AGB stellar model, just before the start of the proton ingestion event. The temperature and density were fixed to 220 MK and 2500 g cm^{-3}, respectively, which are typical values in the pulse of low-metallicity AGB models. The nucleosynthesis was calculated over a total time of 2×10^5 s (~ 2.3 days). To mimic the proton ingestion episode in the one-zone model, an initial abundance of protons was set to 2×10^{-5} and 3×10^{-4} leading to maximum neutron densities of $N_{\rm n,max} = 1.5 \times 10^{14}$ cm^{-3} and 6.7×10^{14} cm^{-3}, respectively. For a low initial proton abundance, a weak i-process develops and elements up to the first peak ($A \lesssim 90$) are synthesized (Fig. 7, black pattern). With more protons, a larger neutron density is reached and elements of the third peak (Fig. 7, red pattern) are produced. For this particular case, the final chemical composition is found to be very similar to that of the full multi-zone AGB model where densities up to $N_n = 2.1 \times 10^{15}$ cm^{-3} are reached.

As shown in Fig. 8, increasing the rate of ^{65}Ni(n,γ) (case 2) leads to a smaller production of ^{65}Cu (as a result of ^{65}Ni decay) by a factor of ~ 3 in both weak and strong i-process cases. Lowering ^{66}Ni(n,γ) (case 3) has the strongest impact since ^{66}Ni now acts as a bottleneck. In the weak i-process case (Fig. 8, top panel), it leads to an overproduction of ^{66}Zn by a factor of ~ 10 to the detriment of $70 < A < 90$ isotopes ($30 < Z < 40$), which are underproduced by a factor of ~ 3 at maximum. For a higher neutron density (Fig. 8, bottom panel), the production of $66 < A < 135$ isotopes ($28 < Z < 54$) is enhanced by a factor of typically $2-4$. The uncertainties on the nominal ^{66}Ni(n,γ) MACS obtained in this work (± 5 mb at 30 keV) induce a variation of about a factor of 3 at $A = 66$ (dashed lines in Fig. 8, top panel).

Ref. [15] investigated the case of a weak i-process using one-zone models with an initial metallicity of [Fe/H] $= -1.6$ ([Fe/H] $= -2.5$ here) and different reaction rates (most of (n,γ) rates coming from the JINA REACLIB library [58]). Although the physical inputs are different, in the case of a weak i-process the results are qualitatively similar to those of Ref. [15] : an underproduction of the elements with $32 < Z < 42$ when adopting a low ^{66}Ni(n,γ) rate.

However, when considering a full multi-zone AGB calculation, the impact of ^{66}Ni(n,γ) is strongly damped (Fig. 9). The overproduction of ^{66}Zn in case 3 is clearly present but the enrichment is a factor of ~ 3 lower. In the stellar model, multiple zones with different temperatures, densities, chemical compositions and irradiations are mixed together by convection leading to a dilute production of the elements, an effect that cannot be captured by one-zone calculations.

The impact of the ^{66}Ni(n,γ) reaction appears to be marginal in low-metallicity AGB stars experiencing i-process nucleosynthesis. It shows that one-zone calculations should be taken with caution. We should also emphasize that only one i-process site was investigated and we cannot exclude a different impact of ^{66}Ni(n,γ) in other sites such as e.g. rapidly accreting white dwarfs [78].

VII. SUMMARY

In this paper we have presented experimental NLD and γSF of the unstable ^{67}Ni nucleus. It is the first time the Oslo method has been applied to an inverse kinematics experiment with a radioactive beam. Due to the lack of reliable nuclear data for ^{67}Ni the NLD and γSF are normalized to model predictions resulting in large uncertainties. Hauser-Feshbach calculations were performed with the extracted NLD and γSF to find the neutron capture cross section of ^{66}Ni. The result of these calculations showed a rather high capture rate compared to the theoretical range, and can help improve our understanding of the i-process nucleosynthesis. In agreement with Ref. [15], we find that the reaction ^{66}Ni(n,γ) acts as bottleneck when using one-zone models. Nevertheless, the impact is strongly damped in multi-zone low-metallicity AGB stellar models experiencing i-process nucleosynthesis. This reaction may however have a different impact in other i-process sites.

ACKNOWLEDGMENTS

The authors would like to thank the accelerator team at CERN ISOLDE for excellent running conditions. This work is based on research supported by the Research Council of Norway under project Grants no. 263030 (V.W.I., S.S., A.G., F.Z., L.C.C.), 325714 (V.W.I, S.S.) and 245882 (P.J., T.L.C., F.B.G.), by the National Research Foundation of South Africa under grant no. 118846, the EU Horizon 2020 research and inno- vation program through ENSAR2 (Grant No. 654002) and the U.S. Department of Energy by Lawrence Livermore National Laboratory under Contract DE-AC52-07NA27344. Funding was provided by the German BMBF under contracts 05P18PKCIA (P.R.), 05P21PKCI1 (N.W.), 05P15RDCIA (T.K.) and 'Verbundprojekt' 05P18PKCI1 (P.R.), 05P18PKCI1 (N.W.). This work was supported by the Fonds de la Recherche Scientifique-FNRS under Grant No IISN 4.4502.19. L.S. and S.G. are senior FRS-F.N.R.S. research associates. G.R. acknowledges the support by the Bulgarian Ministry of Education and Science, within the National Roadmap for Research Infrastructures (object CERN). Supported by the Research Foundation Flanders (FWO, Belgium) under GOA/2015/010 (BOF KU Leuven), and the FWO and F.R.S.-FNRS under the Excellence of Science (EOS) programme (No. 40007501).

Appendix: Shell model level density in Ni isotopes

Fig. 10 and 11 compares the experimental NLD of ^{60,64}Ni [60, 61] and ^{59,63,65,69}Ni [60, 62–64], respectively, with the NLD found in large-scale SM calculations of [31].

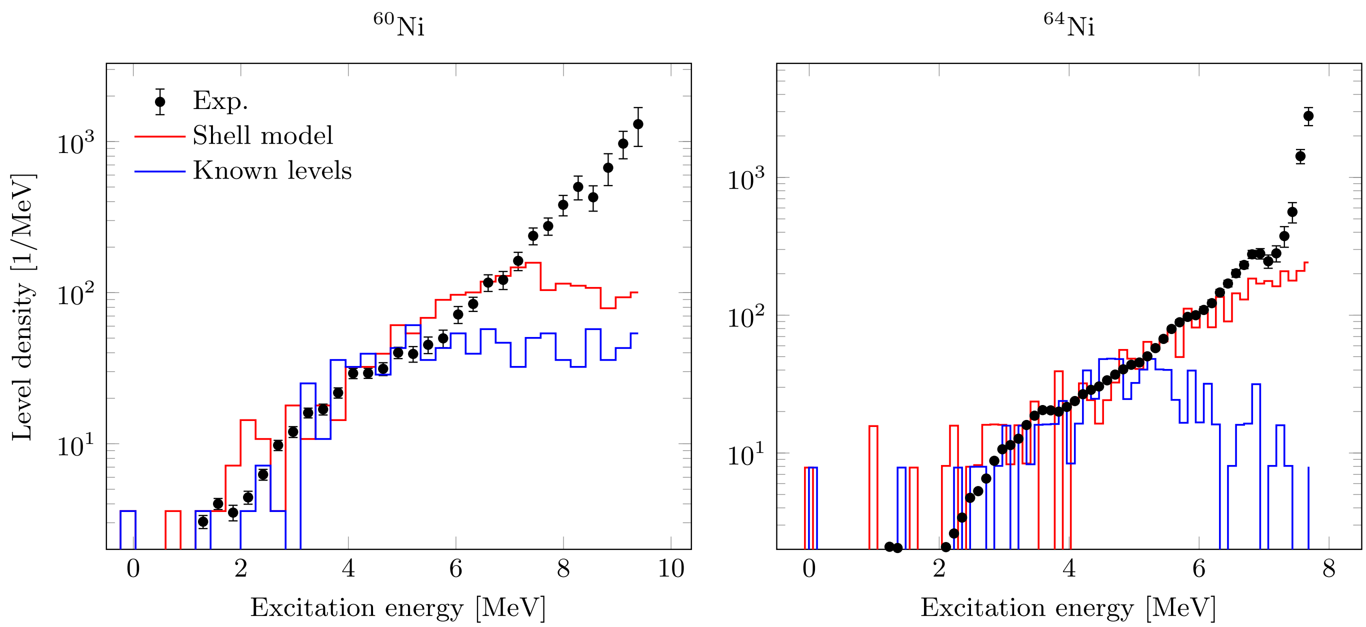

FIG. 10. Measured NLD of even-A Ni nuclei [60, 61] compared with SM calculations from [31].

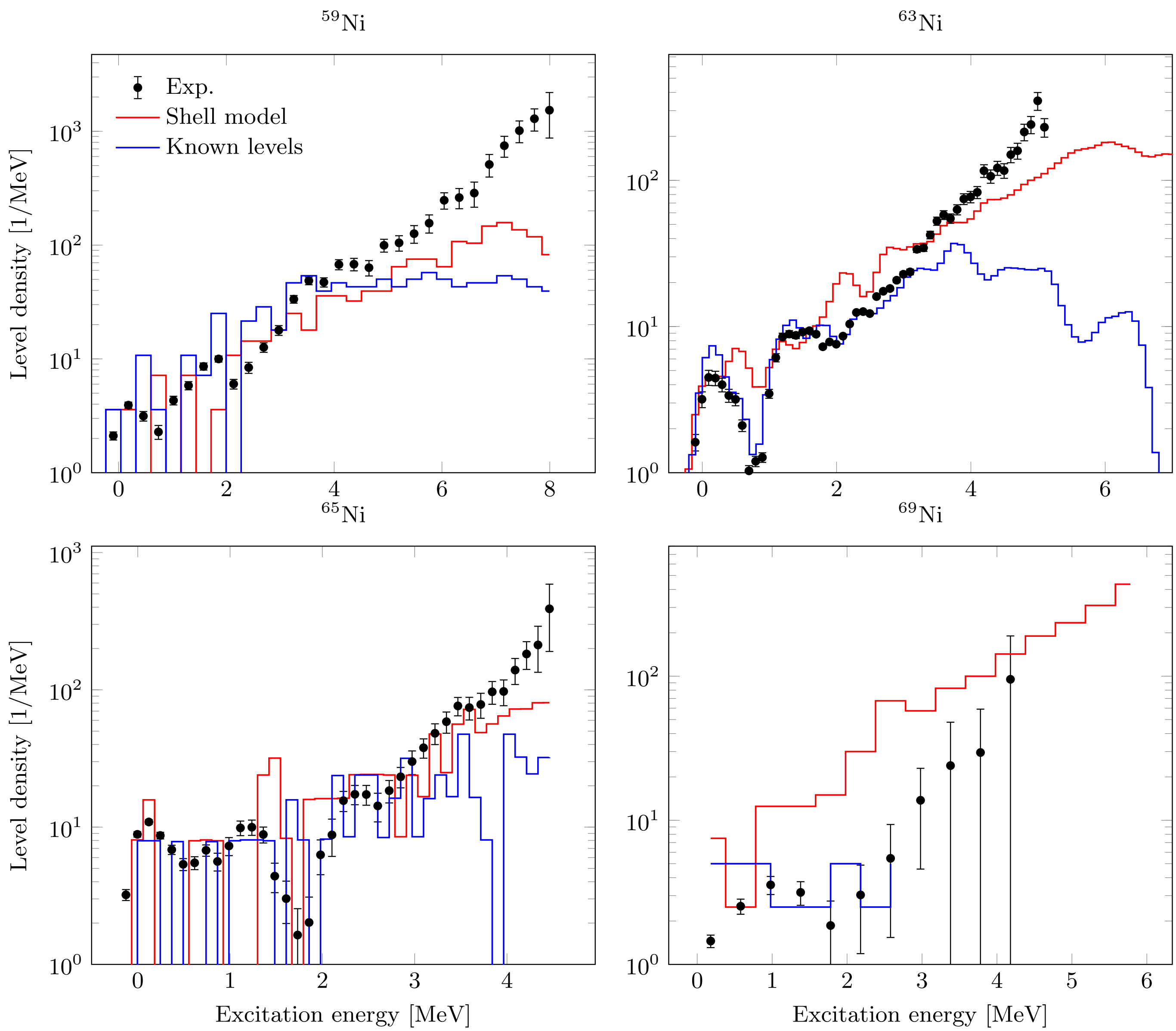

FIG. 11. Measured NLD of odd-A Ni nuclei [60, 62–64] compared with SM calculations with from [31].

[1] P. Merrill, Technetium in the stars, Science **115**, 479 (1952).

[2] E. M. Burbidge, G. R. Burbidge, W. A. Fowler, and F. Hoyle, Synthesis of the elements in stars, Reviews of Modern Physics **29**, 547 (1957).

[3] J. J. Cowan and W. K. Rose, Production of C-14 and neutrons in red giants, The Astrophysical Journal **212**, 149 (1977).

[4] I. U. Roederer, A. I. Karakas, M. Pignatari, and F. Herwig, The Diverse Origines of Neutron-capture Elements in The Metal-poor Star HD 94028: Possible Detection of Products of i-process Nucleosynthesis , The Astrophysical Journal **821**, 37 (2016).

[5] S. Goriely, P. Dimitriou, M. Wiedeking, T. Belgya, R. Firestone, J. Kopecky, M. Krtička, V. Plujko, R. Schwengner, S. Siem, H. Utsunomiya, S. Hilaire, S. Péru, Y. S. Cho, D. M. Filipescu, N. Iwamoto, T. Kawano, V. Varlamov, and R. Xu, Reference database for photon strength functions, European Physical Journal A **55**, 172 (2019).

[6] A. Schiller, L. Bergholt, M. Guttormsen, E. Melby, J. Rekstad, and S. Siem, Extraction of level density and γ strength function from primary γ spectra, Nuclear Instruments and Methods in Physics Research, Section A: Accelerators, Spectrometers, Detectors and Associated Equipment **447**, 498 (2000).

[7] J. E. Midtbø, F. Zeiser, E. Lima, A. C. Larsen, G. M. Tveten, M. Guttormsen, F. L. Bello Garrote, A. Kvellestad, and T. Renstrøm, A new software implementation of the Oslo method with rigorous statistical uncertainty propagation, Computer Physics Communications **262**, 10.1016/j.cpc.2020.107795 (2021).

[8] W. Hauser and H. Feshbach, The Inelastic Scattering of Neutrons, Phys. Rev. **87**, 366 (1952).

[9] A. Spyrou, S. N. Liddick, A. C. Larsen, M. Guttormsen, K. Cooper, A. C. Dombos, D. J. Morrissey, F. Naqvi, G. Perdikakis, S. J. Quinn, T. Renstrøm, J. A. Rodriguez, A. Simon, C. S. Sumithrarachchi, and R. G. Zegers, Novel technique for constraining r -process (n, γ) reaction rates, Physical Review Letters **113**, 232502 (2014).

[10] A. C. Larsen, J. E. Midtbø, M. Guttormsen, T. Renstrøm, S. N. Liddick, A. Spyrou, S. Karampagia, B. A. Brown, O. Achakovskiy, S. Kamerdzhiev, D. L. Bleuel, A. Couture, L. C. Campo, B. P. Crider, A. C. Dombos, R. Lewis, S. Mosby, F. Naqvi, G. Perdikakis, C. J. Prokop, S. J. Quinn, and S. Siem, Enhanced low-energy γ-decay strength of Ni 70 and its robustness within the shell model, Physical Review C **97**, 54329 (2018).

[11] R. Lewis, S. N. Liddick, A. C. Larsen, A. Spyrou, D. L. Bleuel, A. Couture, L. C. Campo, B. P. Crider, A. C. Dombos, M. Guttormsen, S. Mosby, F. Naqvi, G. Perdikakis, C. J. Prokop, S. J. Quinn, T. Renstrøm, and S. Siem, Experimental constraints on the ^{73}Zn$(n,\gamma)^{74}$Zn reaction rate, Physical Review C **99**, 034601 (2019).

[12] S. N. Liddick, A. Spyrou, B. P. Crider, F. Naqvi, A. C. Larsen, M. Guttormsen, M. Mumpower, R. Surman, G. Perdikakis, D. L. Bleuel, A. Couture, L. Crespo Campo, A. C. Dombos, R. Lewis, S. Mosby, S. Nikas, C. J. Prokop, T. Renstrom, B. Rubio, S. Siem, and S. J. Quinn, Experimental Neutron Capture Rate Constraint Far from Stability, Physical Review Letters **116**, 242502 (2016).

[13] S. Liddick, A. Larsen, M. Guttormsen, A. Spyrou, B. Crider, F. Naqvi, J. Midtbø, F. Bello Garrote, D. Bleuel, L. Crespo Campo, A. Couture, A. Dombos, F. Giacoppo, A. Görgen, K. Hadynska-Klek, T. Hagen, V. Ingeberg, B. Kheswa, R. Lewis, S. Mosby, G. Perdikakis, C. Prokop, S. Quinn, T. Renstrøm, S. Rose, E. Sahin, S. Siem, G. Tveten, M. Wiedeking, and F. Zeiser, Benchmarking the extraction of statistical neutron capture cross sections on short-lived nuclei for applications using the β -Oslo method, Physical Review C **100**, 10.1103/PhysRevC.100.024624 (2019).

[14] V. W. Ingeberg, S. Siem, M. Wiedeking, K. Sieja, D. L. Bleuel, C. P. Brits, T. D. Bucher, T. S. Dinoko, J. L. Easton, A. Görgen, M. Guttormsen, P. Jones, B. V. Kheswa, N. A. Khumalo, A. C. Larsen, E. A. Lawrie, J. J. Lawrie, S. N. Majola, K. L. Malatji, L. Makhathini, B. Maqabuka, D. Negi, S. P. Noncolela, P. Papka, E. Sahin, R. Schwengner, G. M. Tveten, F. Zeiser, and B. R. Zikhali, First application of the Oslo method in inverse kinematics, European Physical Journal A **56**, 68 (2020).

[15] J. E. McKay, P. A. Denissenkov, F. Herwig, G. Perdikakis, and H. Schatz, The impact of (n,γ) reaction rate uncertainties on the predicted abundances of i-process elements with 32 ¡= Z ¡= 48 in the metal-poor star HD94028, Monthly Notices of the Royal Astronomical Society **491**, 5179 (2020).

[16] Y. Kadi, M. A. Fraser, and A. Papageorgiou-Koufidou, *HIE-ISOLDE: technical design report for the energy upgrade*, edited by Y. Kadi (CERN, Geneva, 2018).

[17] V. N. Fedoseyev, G. Huber, U. Köster, J. Lettry, V. I. Mishin, H. Ravn, and V. Sebastian, The ISOLDE laser ion source for exotic nuclei, Hyperfine Interactions **127**, 409 (2000).

[18] F. Ames, G. Bollen, P. Delahaye, O. Forstner, G. Huber, O. Kester, K. Reisinger, and P. Schmidt, Cooling of radioactive ions with the Penning trap REXTRAP, Nuclear Instruments and Methods in Physics Research, Section A: Accelerators, Spectrometers, Detectors and Associated Equipment **538**, 17 (2005).

[19] F. Wenander, EBIS as charge breeder for radioactive ion beam accelerators, Nuclear Physics A **701**, 528 (2002).

[20] F. Wenander, Charge breeding of radioactive ions with EBIS and EBIT, Journal of Instrumentation **5** (10), C10004.

[21] N. Kheswa, T. Dinoko, and M. Wiedeking, The production of deuterated polyethylene targets, EPJ Web of Conferences **229**, 03003 (2020).

[22] J. Diriken, N. Patronis, A. Andreyev, S. Antalic, V. Bildstein, A. Blazhev, I. Darby, H. De Witte, J. Eberth, J. Elseviers, V. Fedosseev, F. Flavigny, C. Fransen, G. Georgiev, R. Gernhauser, H. Hess, M. Huyse, J. Jolie, T. Kröll, R. Krücken, R. Lutter, B. Marsh, T. Mertzimekis, D. Muecher, F. Nowacki, R. Orlandi, A. Pakou, R. Raabe, G. Randisi, P. Reiter, T. Roger, M. Seidlitz, M. Seliverstov, K. Sieja, C. Sotty, H. Tornqvist, J. Van De Walle, P. Van Duppen, D. Voulot, N. Warr, F. Wenander, and K. Wimmer, Study of the deformation-driving ν d 5 / 2 orbital in 67 28 Ni 39 using one-neutron transfer

reactions, Physics Letters B **736**, 533 (2014).
[23] S. Hellgartner, D. Mücher, K. Wimmer, V. Bildstein, J. Egido, R. Gernhäuser, R. Krücken, A. Nowak, M. Zielińska, C. Bauer, M. Benito, S. Bottoni, H. De Witte, J. Elseviers, D. Fedorov, F. Flavigny, A. Illana, M. Klintefjord, T. Kröll, R. Lutter, B. Marsh, R. Orlandi, J. Pakarinen, R. Raabe, E. Rapisarda, S. Reichert, P. Reiter, M. Scheck, M. Seidlitz, B. Siebeck, E. Siesling, T. Steinbach, T. Stora, M. Vermeulen, D. Voulot, N. Warr, and F. Wenander, Axial and triaxial degrees of freedom in 72Zn, Physics Letters B **841**, 137933 (2023).
[24] J. Eberth, G. Pascovici, H. G. Thomas, N. Warr, D. Weisshaar, D. Habs, P. Reiter, P. Thirolf, D. Schwalm, C. Gund, H. Scheit, M. Lauer, P. Van Duppen, S. Franchoo, M. Huyse, R. M. Lieder, W. Gast, J. Gerl, and K. P. Lieb, MINIBALL A Ge detector array for radioactive ion beam facilities, Progress in Particle and Nuclear Physics **46**, 389 (2001).
[25] N. Warr, J. Van de Walle, M. Albers, F. Ames, B. Bastin, C. Bauer, V. Bildstein, A. Blazhev, S. Bönig, N. Bree, B. Bruyneel, P. A. Butler, J. Cederkäll, E. Clément, T. E. Cocolios, T. Davinson, H. De Witte, P. Delahaye, D. D. DiJulio, J. Diriken, J. Eberth, A. Ekström, J. Elseviers, S. Emhofer, D. V. Fedorov, V. N. Fedosseev, S. Franchoo, C. Fransen, L. P. Gaffney, J. Gerl, G. Georgiev, R. Gernhäuser, T. Grahn, D. Habs, H. Hess, A. M. Hurst, M. Huyse, O. Ivanov, J. Iwanicki, D. G. Jenkins, J. Jolie, N. Kesteloot, O. Kester, U. Köster, M. Krauth, T. Kröll, R. Krücken, M. Lauer, J. Leske, K. P. Lieb, R. Lutter, L. Maier, B. A. Marsh, D. Mücher, M. Münch, O. Niedermaier, J. Pakarinen, M. Pantea, G. Pascovici, N. Patronis, D. Pauwels, A. Petts, N. Pietralla, R. Raabe, E. Rapisarda, P. Reiter, A. Richter, O. Schaile, M. Scheck, H. Scheit, G. Schrieder, D. Schwalm, M. Seidlitz, M. Seliverstov, T. Sieber, H. Simon, K. H. Speidel, C. Stahl, I. Stefanescu, P. G. Thirolf, H. G. Thomas, M. Thürauf, P. Van Duppen, D. Voulot, R. Wadsworth, G. Walter, D. Weißhaar, F. Wenander, A. Wiens, K. Wimmer, B. H. Wolf, P. J. Woods, K. Wrzosek-Lipska, and K. O. Zell, The Miniball spectrometer, The European Physical Journal A **49**, 40 (2013).
[26] M. Guttormsen, T. S. Tveter, L. Bergholt, F. Ingebretsen, and J. Rekstad, The unfolding of continuum γ-ray spectra, Nuclear Instruments and Methods in Physics Research, Section A: Accelerators, Spectrometers, Detectors and Associated Equipment **374**, 371 (1996).
[27] S. Agostinelli, J. Allison, K. Amako, J. Apostolakis, H. Araujo, P. Arce, M. Asai, D. Axen, S. Banerjee, G. Barrand, F. Behner, L. Bellagamba, J. Boudreau, L. Broglia, A. Brunengo, H. Burkhardt, S. Chauvie, J. Chuma, R. Chytracek, G. Cooperman, G. Cosmo, P. Degtyarenko, A. Dell'Acqua, G. Depaola, D. Dietrich, R. Enami, A. Feliciello, C. Ferguson, H. Fesefeldt, G. Folger, F. Foppiano, A. Forti, S. Garelli, S. Giani, R. Giannitrapani, D. Gibin, J. J. G. Cadenas, I. González, G. G. Abril, G. Greeniaus, W. Greiner, V. Grichine, A. Grossheim, S. Guatelli, P. Gumplinger, R. Hamatsu, K. Hashimoto, H. Hasui, A. Heikkinen, A. Howard, V. Ivanchenko, A. Johnson, F. W. Jones, J. Kallenbach, N. Kanaya, M. Kawabata, Y. Kawabata, M. Kawaguti, S. Kelner, P. Kent, A. Kimura, T. Kodama, R. Kokoulin, M. Kossov, H. Kurashige, E. Lamanna, T. Lampén, V. Lara, V. Lefebure, F. Lei, M. Liendl, W. Lockman, F. Longo, S. Magni, M. Maire, E. Medernach, K. Minamimoto, P. M. de Freitas, Y. Morita, K. Murakami, M. Nagamatu, R. Nartallo, P. Nieminen, T. Nishimura, K. Ohtsubo, M. Okamura, S. O'Neale, Y. Oohata, K. Paech, J. Perl, A. Pfeiffer, M. G. Pia, F. Ranjard, A. Rybin, S. Sadilov, E. D. Salvo, G. Santin, T. Sasaki, N. Savvas, Y. Sawada, S. Scherer, S. Sei, V. Sirotenko, D. Smith, N. Starkov, H. Stoecker, J. Sulkimo, M. Takahata, S. Tanaka, E. Tcherniaev, E. S. Tehrani, M. Tropeano, P. Truscott, H. Uno, L. Urban, P. Urban, M. Verderi, A. Walkden, W. Wander, H. Weber, J. P. Wellisch, T. Wenaus, D. C. Williams, D. Wright, T. Yamada, H. Yoshida, and D. Zschiesche, Geant4—a simulation toolkit, Nuclear Instruments and Methods in Physics Research Section A: Accelerators, Spectrometers, Detectors and Associated Equipment **506**, 250 (2003).
[28] V. W. Ingeberg, vetlewi/MiniballREX: Ni67 (2022).
[29] M. Guttormsen, T. Ramsøy, and J. Rekstad, The first generation of γ-rays from hot nuclei, Nuclear Inst. and Methods in Physics Research, A **255**, 518 (1987).
[30] A. C. Larsen, M. Guttormsen, M. Krtička, E. Běták, A. Bürger, A. Görgen, H. T. Nyhus, J. Rekstad, A. Schiller, S. Siem, H. K. Toft, G. M. Tveten, A. V. Voinov, and K. Wikan, Analysis of possible systematic errors in the Oslo method, Phys. Rev. C **83**, 34315 (2011).
[31] J. E. Midtbø, A. C. Larsen, T. Renstrøm, F. L. Bello Garrote, and E. Lima, Consolidating the concept of low-energy magnetic dipole decay radiation, Physical Review C **98**, 064321 (2018).
[32] F. Feroz and M. P. Hobson, Multimodal nested sampling: an efficient and robust alternative to Markov Chain Monte Carlo methods for astronomical data analyses, Monthly Notices of the Royal Astronomical Society **384**, 449 (2008).
[33] F. Feroz, M. P. Hobson, and M. Bridges, MultiNest: an efficient and robust Bayesian inference tool for cosmology and particle physics, Monthly Notices of the Royal Astronomical Society **398**, 1601 (2009).
[34] F. Feroz, M. P. Hobson, E. Cameron, and A. N. Pettitt, Importance Nested Sampling and the MultiNest Algorithm, The Open Journal of Astrophysics **2**, 10.21105/astro.1306.2144 (2019).
[35] J. Buchner, A. Georgakakis, K. Nandra, L. Hsu, C. Rangel, M. Brightman, A. Merloni, M. Salvato, J. Donley, and D. Kocevski, X-ray spectral modelling of the AGN obscuring region in the CDFS: Bayesian model selection and catalogue, Astronomy & Astrophysics **564**, A125 (2014).
[36] H. A. Bethe, An Attempt to Calculate the Number of Energy Levels of a Heavy Nucleus, Phys. Rev. **50**, 332 (1936).
[37] A. Gilbert and A. G. W. Cameron, a Composite Nuclear-Level Density Formula With Shell Corrections, Canadian Journal of Physics **43**, 1446 (1965).
[38] T. Ericson, A statistical analysis of excited nuclear states, Nuclear Physics **11**, 481 (1959).
[39] S. Goriely, S. Hilaire, and A. J. Koning, Improved microscopic nuclear level densities within the Hartree-Fock-Bogoliubov plus combinatorial method, Physical Review C - Nuclear Physics **78**, 64307 (2008).
[40] R. Capote, M. Herman, P. Obložinský, P. G. Young, S. Goriely, T. Belgya, A. V. Ignatyuk, A. J. Koning, S. Hilaire, V. A. Plujko, M. Avrigeanu, O. Bersillon,

M. B. Chadwick, T. Fukahori, Z. Ge, Y. Han, S. Kailas, J. Kopecky, V. M. Maslov, G. Reffo, M. Sin, E. S. Soukhovitskii, and P. Talou, RIPL - Reference Input Parameter Library for Calculation of Nuclear Reactions and Nuclear Data Evaluations, Nuclear Data Sheets **110**, 3107 (2009).

[41] M. Guttormsen, S. Goriely, A. C. Larsen, A. Görgen, T. W. Hagen, T. Renstrøm, S. Siem, N. U. Syed, G. Tagliente, H. K. Toft, H. Utsunomiya, A. V. Voinov, and K. Wikan, Quasicontinuum γ decay of Zr 91,92: Benchmarking indirect (n,γ) cross section measurements for the s process, Physical Review C **96**, 24313 (2017).

[42] S. Goriely and V. Plujko, Simple empirical E1 and M1 strength functions for practical applications, Physical Review C **99**, 14303 (2019).

[43] S. Goriely, S. Hilaire, S. Péru, and K. Sieja, Gogny-HFB+QRPA dipole strength function and its application to radiative nucleon capture cross section, Physical Review C **98**, 014327 (2018).

[44] S. Hilaire and M. Girod, Large-scale mean-field calculations from proton to neutron drip lines using the D1S Gogny force, The European Physical Journal A **33**, 237 (2007).

[45] R. Schwengner, S. Frauendorf, and A. C. Larsen, Low-Energy Enhancement of Magnetic Dipole Radiation, Phys. Rev. Lett. **111**, 232504 (2013).

[46] S. Frauendorf and R. Schwengner, Evolution of low-lying M1 modes in germanium isotopes, Physical Review C **105**, 034335 (2022).

[47] B. A. Brown and A. C. Larsen, Large low-energy M1 strength for Fe 56,57 within the nuclear shell model, Physical Review Letters **113**, 252502 (2014).

[48] K. Sieja, Electric and Magnetic Dipole Strength at Low Energy, Phys. Rev. Lett. **119**, 52502 (2017).

[49] D. M. Rossi, P. Adrich, F. Aksouh, H. Alvarez-Pol, T. Aumann, J. Benlliure, M. Böhmer, K. Boretzky, E. Casarejos, M. Chartier, A. Chatillon, D. Cortina-Gil, U. Datta Pramanik, H. Emling, O. Ershova, B. Fernandez-Dominguez, H. Geissel, M. Gorska, M. Heil, H. T. Johansson, A. Junghans, A. Kelic-Heil, O. Kiselev, A. Klimkiewicz, J. V. Kratz, R. Krücken, N. Kurz, M. Labiche, T. Le Bleis, R. Lemmon, Y. A. Litvinov, K. Mahata, P. Maierbeck, A. Movsesyan, T. Nilsson, C. Nociforo, R. Palit, S. Paschalis, R. Plag, R. Reifarth, D. Savran, H. Scheit, H. Simon, K. Sümmerer, A. Wagner, W. Walua, H. Weick, and M. Winkler, Measurement of the dipole polarizability of the unstable neutron-rich nucleus Ni68, Physical Review Letters **111**, 242503 (2013).

[50] T. Von Egidy, H. H. Schmidt, and A. N. Behkami, Nuclear level densities and level spacing distributions: Part II, Nuclear Physics, Section A **481**, 189 (1988).

[51] T. v. Egidy and D. Bucurescu, Systematics of nuclear level density parameters, Physical Review C **72**, 044311 (2005).

[52] T. von Egidy and D. Bucurescu, Experimental energy-dependent nuclear spin distributions, Phys. Rev. C **80**, 54310 (2009).

[53] H. Junde, H. Xiaolong, and J. K. Tuli, Nuclear Data Sheets for A = 67, Nuclear Data Sheets **106**, 159 (2005).

[54] J. Diriken, N. Patronis, A. Andreyev, S. Antalic, V. Bildstein, A. Blazhev, I. G. Darby, H. De Witte, J. Eberth, J. Elseviers, V. N. Fedosseev, F. Flavigny, C. Fransen, G. Georgiev, R. Gernhauser, H. Hess, M. Huyse, J. Jolie, T. Kröll, R. Krücken, R. Lutter, B. A. Marsh, T. Mertzimekis, D. Muecher, R. Orlandi, A. Pakou, R. Raabe, G. Randisi, P. Reiter, T. Roger, M. Seidlitz, M. Seliverstov, C. Sotty, H. Tornqvist, J. Van De Walle, P. Van Duppen, D. Voulot, N. Warr, F. Wenander, and K. Wimmer, Experimental study of the 66Ni(d, p) 67Ni one-neutron transfer reaction, Physical Review C - Nuclear Physics **91**, 54321 (2015).

[55] A. J. Koning, S. Hilaire, and M. C. Duijvestijn, TALYS-1.0, in *ND2007* (EDP Sciences, Les Ulis, France, 2007) pp. 211–214.

[56] A. Koning, D. Rochman, J.-C. Sublet, N. Dzysiuk, M. Fleming, and S. van der Marck, TENDL: Complete Nuclear Data Library for Innovative Nuclear Science and Technology, Nuclear Data Sheets **155**, 1 (2019).

[57] A. J. M. Plompen, O. Cabellos, C. De Saint Jean, M. Fleming, A. Algora, M. Angelone, P. Archier, E. Bauge, O. Bersillon, A. Blokhin, F. Cantargi, A. Chebboubi, C. Diez, H. Duarte, E. Dupont, J. Dyrda, B. Erasmus, L. Fiorito, U. Fischer, D. Flammini, D. Foligno, M. R. Gilbert, J. R. Granada, W. Haeck, F.-J. Hambsch, P. Helgesson, S. Hilaire, I. Hill, M. Hursin, R. Ichou, R. Jacqmin, B. Jansky, C. Jouanne, M. A. Kellett, D. H. Kim, H. I. Kim, I. Kodeli, A. J. Koning, A. Y. Konobeyev, S. Kopecky, B. Kos, A. Krása, L. C. Leal, N. Leclaire, P. Leconte, Y. O. Lee, H. Leeb, O. Litaize, M. Majerle, J. I. Márquez Damián, F. Michel-Sendis, R. W. Mills, B. Morillon, G. Noguère, M. Pecchia, S. Pelloni, P. Pereslavtsev, R. J. Perry, D. Rochman, A. Röhrmoser, P. Romain, P. Romojaro, D. Roubtsov, P. Sauvan, P. Schillebeeckx, K. H. Schmidt, O. Serot, S. Simakov, I. Sirakov, H. Sjöstrand, A. Stankovskiy, J. C. Sublet, P. Tamagno, A. Trkov, S. van der Marck, F. Álvarez-Velarde, R. Villari, T. C. Ware, K. Yokoyama, and G. Žerovnik, The joint evaluated fission and fusion nuclear data library, JEFF-3.3, The European Physical Journal A **56**, 181 (2020).

[58] R. H. Cyburt, A. M. Amthor, R. Ferguson, Z. Meisel, K. Smith, S. Warren, A. Heger, R. D. Hoffman, T. Rauscher, A. Sakharuk, H. Schatz, F. K. Thielemann, and M. Wiescher, The jina reaclib database: Its recent updates and impact on type-i x-ray bursts, The Astrophysical Journal Supplement Series **189**, 240 (2010).

[59] M. Arnould and S. Goriely, Microscopic nuclear models for astrophysics: The brussels bruslib nuclear library and beyond, Nucl. Phys. A **777**, 157 (2006).

[60] H. Utsunomiya, T. Renstrøm, G. M. Tveten, S. Goriely, S. Katayama, T. Ari-Izumi, D. Takenaka, D. Symochko, B. V. Kheswa, V. W. Ingeberg, T. Glodariu, Y. W. Lui, S. Miyamoto, A. C. Larsen, J. E. Midtbø, A. Görgen, S. Siem, L. C. Campo, M. Guttormsen, S. Hilaire, S. Péru, and A. J. Koning, Photoneutron cross sections for Ni isotopes: Toward understanding (n,γ) cross sections relevant to weak s -process nucleosynthesis, Physical Review C **98**, 54619 (2018).

[61] L. Crespo Campo, F. L. Bello Garrote, T. K. Eriksen, A. Görgen, M. Guttormsen, K. Hadynska-Klek, M. Klintefjord, A. C. Larsen, T. Renstrøm, E. Sahin, S. Siem, A. Springer, T. G. Tornyi, and G. M. Tveten, Statistical γ -decay properties of Ni 64 and deduced (n,γ) cross section of the s -process branch-point nucleus Ni 63, Physical Review C **94**, 44321 (2016).

[62] V. W. Ingeberg, P. Jones, L. Msebi, S. Siem, M. Wiedeking, A. A. Avaa, M. V. Chisapi, E. A. Lawrie, K. L.

Malatji, L. Makhathini, S. P. Noncolela, and O. Shirinda, Nuclear level density and γ-ray strength function of ^{63}Ni, Phys. Rev. C **106**, 054315 (2022).

[63] L. C. Campo, A. C. Larsen, F. L. Garrote, T. K. Eriksen, F. Giacoppo, A. Görgen, M. Guttormsen, M. Klintefjord, T. Renstrøm, E. Sahin, S. Siem, T. G. Tornyi, and G. M. Tveten, Investigating the γ decay of Ni 65 from particle-γ coincidence data, Physical Review C **96**, 14312 (2017).

[64] A. Spyrou, A. C. Larsen, S. N. Liddick, F. Naqvi, B. P. Crider, A. C. Dombos, M. Guttormsen, D. L. Bleuel, A. Couture, L. C. Campo, R. Lewis, S. Mosby, M. R. Mumpower, G. Perdikakis, C. J. Prokop, S. J. Quinn, T. Renstrom, S. Siem, and R. Surman, Neutron-capture rates for explosive nucleosynthesis: The case of 68Ni(n, γ)69Ni, Journal of Physics G: Nuclear and Particle Physics **44**, 044002 (2017).

[65] R. Schwengner, S. Frauendorf, and B. Brown, Low-Energy Magnetic Dipole Radiation in Open-Shell Nuclei, Physical Review Letters **118**, 092502 (2017).

[66] M. Guttormsen, K. O. Ay, M. Ozgur, E. Algin, A. C. Larsen, F. L. Bello Garrote, H. C. Berg, L. Crespo Campo, T. Dahl-Jacobsen, F. W. Furmyr, D. Gjestvang, A. Görgen, T. W. Hagen, V. W. Ingeberg, B. V. Kheswa, I. K. B. Kullmann, M. Klintefjord, M. Markova, J. E. Midtbø, V. Modamio, W. Paulsen, L. G. Pedersen, T. Renstrøm, E. Sahin, S. Siem, G. M. Tveten, and M. Wiedeking, Evolution of the γ-ray strength function in neodymium isotopes, Phys. Rev. C **106**, 034314 (2022).

[67] N. Iwamoto, T. Kajino, G. J. Mathews, M. Y. Fujimoto, and W. Aoki, Flash-Driven Convective Mixing in Low-Mass, Metal-deficient Asymptotic Giant Branch Stars: A New Paradigm for Lithium Enrichment and a Possible s-Process, Astrophys. J. **602**, 377 (2004).

[68] S. Cristallo, L. Piersanti, O. Straniero, R. Gallino, I. Domínguez, and F. Käppeler, Asymptotic-Giant-Branch Models at Very Low Metallicity, Publications of the Astronomical Society of Australia **26**, 139 (2009), arXiv:0904.4173 [astro-ph.SR].

[69] T. Suda and M. Y. Fujimoto, Evolution of low- and intermediate-mass stars with [Fe/H] ¡= - 2.5, Monthly Notices of the Royal Astronomical Society **405**, 177 (2010), arXiv:1002.0863 [astro-ph.GA].

[70] R. J. Stancliffe, D. S. P. Dearborn, J. C. Lattanzio, S. A. Heap, and S. W. Campbell, Three-dimensional Hydrodynamical Simulations of a Proton Ingestion Episode in a Low-metallicity Asymptotic Giant Branch Star, Astrophys. J. **742**, 121 (2011), arXiv:1109.1289 [astro-ph.SR].

[71] A. Choplin, L. Siess, and S. Goriely, The intermediate neutron capture process. I. Development of the i-process in low-metallicity low-mass AGB stars, Astronomy & Astrophysics **648**, A119 (2021), arXiv:2102.08840 [astro-ph.SR].

[72] L. Siess, E. Dufour, and M. Forestini, An internet server for pre-main sequence tracks of low- and intermediate-mass stars, Astronomy & Astrophysics **358**, 593 (2000).

[73] L. Siess, Evolution of massive AGB stars. I. Carbon burning phase, Astronomy & Astrophysics **448**, 717 (2006).

[74] S. Goriely and L. Siess, Sensitivity of the s-process nucleosynthesis in agb stars to the overshoot model, Astronomy & Astrophysics **609**, A29 (2018).

[75] Y. Xu, S. Goriely, A. Jorissen, G. Chen, and M. Arnould, Databases and tools for nuclear astrophysics applications: Brussels nuclear library (bruslib), nuclear astrophysics compilation of reactions ii (nacre ii) and nuclear network generator (netgen), Astronomy & Astrophysics **549**, 10 (2013), A106.

[76] S. Goriely, L. Siess, and A. Choplin, The intermediate neutron capture process. II. Nuclear uncertainties, Astronomy & Astrophysics **654**, A129 (2021), arXiv:2109.00332 [astro-ph.SR].

[77] A. Choplin, L. Siess, and S. Goriely, The intermediate neutron capture process. III. The i-process in AGB stars of different masses and metallicities without overshoot, Astronomy & Astrophysics **667**, A155 (2022), arXiv:2209.10303 [astro-ph.SR].

[78] P. A. Denissenkov, F. Herwig, U. Battino, C. Ritter, M. Pignatari, S. Jones, and B. Paxton, I-process Nucleosynthesis and Mass Retention Efficiency in He-shell Flash Evolution of Rapidly Accreting White Dwarfs, Astrophysical Journal, Letters **834**, L10 (2017), arXiv:1610.08541 [astro-ph.SR].